Solar-Terrestrial Physics. 2022. Vol. 8. Iss. 1. P. 10–19. DOI: 10.12737/stp-82202202. © 2022
V.G. Eselevich, M.V. Eselevich, I.V. Zimovets. Published by INFRA-M Academic Publishing House

UDC 523.98
DOI: 10.12737/stp-82202202

Received December 16, 2021
Accepted February 28, 2022

POSSIBLE DIFFERENCE IN THE FORMATION OF CORONAL MASS EJECTIONS OF TWO TYPES

V.G. Eselevich
Institute of Solar-Terrestrial Physics SB RAS, Irkutsk, Russia, esel@iszf.irk.ru

M.V. Eselevich
Institute of Solar-Terrestrial Physics SB RAS, Irkutsk, Russia, mesel@iszf.irk.ru

I.V. Zimovets
Space Research Institute RAS, Moscow, Russia, ivanzim@iki.rssi.ru

Abstract. Analysis of seven near-limb coronal mass ejections (CMEs) has shown that at distances $R<1.4R_\odot$ from the center of the Sun CMEs according to their formation can be divided into two types: type 1 CMEs and type 2 CMEs. In the case of type 1 CMEs, the frontal structure (FS) is formed by processes occurring in FS itself, which is the outer shell of the magnetic flux rope. As for type 2 CMEs, EP-CME, internal arched structures erupt, explosively expand, capture, and accelerate the more distant arched structures, which merge to form the frontal structure of the type 2 CMEs.

Keywords: coronal mass ejection, magnetic flux rope, coronal arched structures, flare, eruptive prominence.

INTRODUCTION

Experimental studies and various simulation methods have made it possible to fairly reliably establish that coronal mass ejections (CMEs) are a plasma-filled magnetic flux rope with footpoints in the photosphere [Krall et al., 2000; Thernisien et al., 2009]. The outer shell of magnetic flux rope is called the frontal structure (FS) of CME. Note that the magnetic flux rope as a magnetic flux tube has an additional magnetic field component perpendicular to the main longitudinal field of the tube.

Sheeley et al. [1999] by kinematic characteristics have classified CMEs into two groups: gradual (slowly evolving) and impulsive. For the first time such a classification of CMEs, but under other names (eruption-associated and flare-associated), was made in [MacQueen, Fisher, 1983]. According to [Sheeley et al., 1999], gradual CMEs are associated with prominence eruption and reach maximum velocities V_{max}=400÷600 km/s, whereas impulsive CMEs are related to solar flares and have V_{max}>750 km/s.

Gradual CMEs are formed in the corona at heights of 0.1 $R_\odot<h<1.0R_\odot$($R_\odot$ is the solar radius) relative to the solar surface. They start moving from a quiescent state, having an angular size 15°–65° [Hundhausen, 1999; Sheeley et al., 1999; Bemporad et al., 2007; Eselevich, Eselevich, 2011]. Patsourakos et al. [2013] managed for the first time to observe and study in detail the development of a magnetic flux rope of a gradual CME (July 19, 2012) on the limb, which was formed above an active region at a low height $h<0.2\ R_\odot$ relative to the solar surface. As a result of these studies, the formation of gradual CMEs is pictured as follows. There is a magnetic flux rope in the corona, which is filled with plasma and has footpoints in the photosphere. Due to the development of instability, it can erupt, i.e. be ejected in a direction away from the Sun. The type of instability leading to the eruption and causes of its development remain unclear despite a number of researchers have proposed its mechanisms [Antiochos et al., 1999; Amari et al., 2000; Magara, Longcope, 2001; Gibson et al., 2006; Archontis and Hood, 2008].

The question of how a magnetic flux rope is formed in the corona before eruption still remains open. One of today's most widely accepted theories attributes its occurrence to the so-called tether-cutting magnetic reconnection [Moore et al., 2001]. During this process, the system of crossed magnetic loops with shear reconnects above the photospheric polarity inversion line. This leads to the formation of a flux rope and its subsequent eruption. A physical cause is an increase in the poloidal magnetic field component and a decrease in the magnetic tension restraining effect. The tether-cutting model is confirmed by a number of observations and numerical calculations (e.g., [Zhang et al., 2001; Sterling, Moore, 2005; Chen et al., 2014; Sharykin et al., 2020]). Also under discussion is the possibility of contribution of kink [Kliem et al., 2004; Shen et al., 2012] and toroidal [Kliem, Török, 2006] instabilities to the eruption.

According to [Schmieder et al., 2013], more than 80 % of all observable eruptions of solar filaments, which in fact are also magnetic flux ropes, become triggers of CMEs.

Impulsive CMEs can be formed either near the solar surface or under the photosphere. The radial velocity of such magnetic flux ropes near the photosphere may be as high as tens to hundreds of kilometers per second, and the minimum angular size is ~1° [Eselevich, Eselevich, 2011].

One of the possible causes of their formation is assumed to be the ejection of a magnetic flux rope, filled with relatively cold plasma, from the convective zone. This possibility has been predicted within the theory of thin magnetic flux tubes as a result of the development

This is an open access article under the CC BY-NC-ND license

of slow wave instability, or Parker instability [Moreno-Insertis et al., 1992; Alekseenko et al., 2000; Romanov et al., 1993a]. The main qualitative conclusions of the theory and their first comparison with experimental data are presented in [Romanov et al., 1993b; Eselevich et al., 2013; Eselevich, Eselevich, 2014]. To directly prove the occurrence of ejection of magnetic flux tubes from the convective zone, which form CMEs of this type, requires measuring the solar magnetic field with a time resolution ~1–10 s, which cannot be made with modern magnetographs: for example, SDO/HMI and SOHO/MDI have a resolution of the order of 1 min.

The classification of CMEs into gradual and impulsive is, however, not supported by statistical studies analyzing a large number of events [Vršnak et al., 2005; Zhang and Dere 2006]. In particular, Vršnak et al. [2005] have carried out a statistical analysis of 545 CMEs associated with flares (flare associated CMEs denoted as F-CMEs) and 104 CMEs associated with eruptive prominences (disappearing filament CMEs designated as DSF-CME or EP-CME) observed at distances $(2\div30)R_\odot$ from the center of the Sun. Both datasets give quite similar characteristics, which contradicts the concept of two different CME types.

The following question arises: if there is no classificatiohn of CMEs into gradual (or EP-CMEs) and impulsive (or F-CMEs), does this mean that all CMEs have the same formation mechanism or there is another classification of CMEs?

This paper is an attempt to answer this fundamental question. For this purpose, we have examined the dynamics at the stage of formation of these two CMEs we designate as type 1 CMEs and type 2 CMEs. Using seven limb CMEs as an example, we analyzed the dependence of the maximum velocity V_b of the CME leading part, observed in the SDO/AIA field of view at distances $R<1.4R_\odot$ from the center of the Sun, on characteristics (features) of the initial stage of CME formation, and, first of all, on the distance R_b of the place of formation of the CME leading part from the center of the Sun.

1. DATA AND ANALYSIS METHODS

Most events have been analyzed using SDO/AIA EUV images in the 131, 193, and 1700 Å channels [Lemen et al., 2012]. The channels were chosen from considerations of the best reflection of the initial stage of CME formation in the images. The time interval between SDO/AIA images is ≈12 s, the spatial resolution is 1.2″ (two pixels) that corresponds to 0.00125 $R_\odot$. The instrument's field of view is up to ≈1.4 $R_\odot$.

The images in the EUV channels were presented as images in the difference brightness with a fixed initial time $\Delta P=P(t)–P(t_0)$, where $P(t_0)$ is the undisturbed brightness at t_0 before the occurrence of the event under study; $P(t)$ is the disturbed brightness at any time $t>t_0$. We used the difference images to explore the CME dynamics. To do this, we plotted distributions of $\Delta P(R)$ relative to the solar center along the radius at a fixed position angle PA at different points of time. The position angle PA is measured in solar images from the north pole counterclockwise. In some cases, we used images in running difference brightness $\Delta P_R=P(t_i)–P(t_{i-1})$, i.e. constructed from two images closest in time.

2. DEPENDENCE OF TYPE 1 CME VELOCITY ON THE DISTANCE R_b, WHERE ITS LEADING PART IS FORMED, RELATIVE TO THE CENTER OF THE SUN

Our study relies on the aforementioned proposition that CMEs originate from the magnetic flux rope whose footpoints are in the photosphere. In this case, we use only limb CMEs that emerge at longitudes >75°–80°. We have analyzed five type 1 CMEs in which filament eruption is either absent or minor. We are interested in how the maximum velocity $V_{b\ max}$ of the type 1 CME leading part, observed in the SDO/AIA field of view at $R<1.4R_\odot$ from the center of the Sun, depends on characteristics and features of the initial stage of type 1 CME formation. These characteristics include the location R_{FS} of the maximum difference brightness ΔP_{FS} of the CME frontal structure (FS) relative to the center of the Sun; the period of time Δt_{FS} during which ΔP_{FS} remains unchanged; space and time features of the dynamics of the CME leading part location R_b and velocity V_b. In addition, we show the type 1 CME leading part velocity V_{av} linearly averaged over distances $3R_\odot<R<30\ R_\odot$, derived from LASCO C2 and C3 coronograph data [http://cdaw.gsfc.nasa.gov/CME_list].

Table presents data on the five type 1 CMEs. Let us examine in detail features of the formation and development of type 1 CMEs, using the January 27, 2012 and July 19, 2012 events as an example. In the former event, the FS leading part was formed closest to the solar surface; in the latter, farthest from it.

2.1. Type 1 CME in the January 27, 2012 event

Let us consider the type 1 CME occurring on January 27, 2012, whose FS was formed closest to the solar surface. Figure 1 presents difference brightness images (at t_0=17:30:11 UT) of the development of this CME in the hot ($T\approx10^7$ K) channel 131 Å for successive time points. What is most noticeable in this channel is the initial stage of the development of the event that occurred in the active region NOAA 11402 and was accompanied by an X1.7 X-ray flare with heliographic coordinates N29W86, which began at ≈17:37 UT. At 17:38:35 and 17:39:23 UT (Figure 1, *a*, *b*), we can see an external arched structure, which is the basis for the future FS, and two internal structures S1 and S2 located below.

Referring to Figure 11 from [Patsourakos et al., 2013], as three-dimensional the observed set of loop-like structures in the plane of the sky is a magnetic flux rope filled with plasma, whose footpoints are in the photosphere. In response to the development of instability, the flux rope can erupt. With time the brightness of structures S1, S2, and FS is enhanced. After 17:39:23 UT (Figure 1, *b*), FS begins to move away from the Sun, i.e. an eruption starts (Figure 1*c*, *d*).

Date and time (UT) of flare maximum in soft X-ray	Heliographic coordinates and X-ray class of flare	Linear-averaged CME velocity V_{av}, km/s	$R_b/R_\odot$	$R_{FS}/R_\odot$	Δt_{FS}, min	$V_{b\ max}$, km/s ($R_b/R_\odot$)	Effect of prominence eruption
June 23, 2012 07:50	N14W89 C2.7	1263	1.105	1.097	8	377 (1.34)	–
July 19, 2012 05:58	S13W88 M7.7	1631	1.213	1.187	10	102 (1.267)	–
September 22, 2011 11:01	N09E89 X1.4	1905	1.09	1.083	5	526 (1.27)	–
January 27, 2012 18:37	N29W86 X1.7	2508	1.037	1.028	4	680 (1.33)	–
September 10, 2017 16:06	S08W88 X8.2	3163	1.024	1.019	1	928 (1.245)	–
August 24., 2014 12:17	S07E78 M5.9	551	1.22	1.19	<1	550 (1.25)	+
February 25, 2014 00:49	S12E82 X4.9	2147	1.165	1.157	3.5±1	2030 (1.24)	+

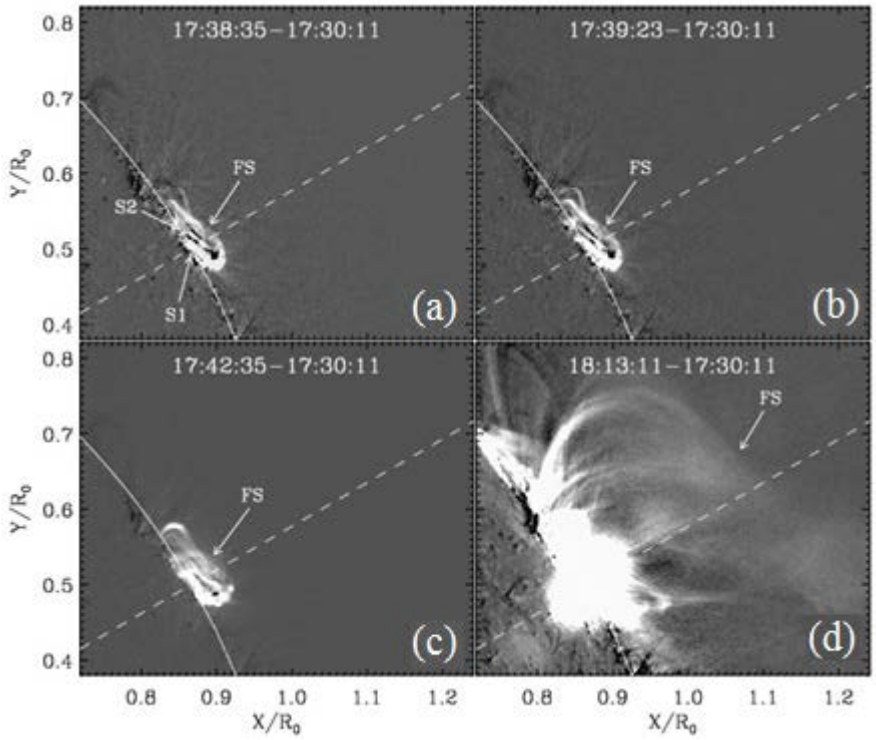

Figure 1. Difference brightness images of the development of type 1 CMEs for successive instants of time on January 27, 2012 (131 Å channel, SDO/AIA data). Positive estimate from the center of the Sun along the Y-axis is to the north, along the X axis, to the west. The distances are normalized to the solar radius $R_\odot$. The dashed line indicates the direction *PA*=300°

Despite an overexposure of AIA/SDO CCD sensors and brightness distortion in the flare area, we can try to analyze the dynamics of this event. For this purpose, we have plotted distributions of difference brightness $\Delta P = P(t) - P(t_0)$ (at t_0=17:30:11 UT) as a function of the distance R from the center of the Sun (Figure 2). The distributions are plotted in the direction of the position angle *PA*=300°. Figure 2, *a* shows that between 17:33:47 (open circles) and 17:38:59 UT (solid circles) the difference brightness of the structures S1, S2, and FS increases to ΔP_1, ΔP_2, and ΔP_{FS} respectively. Their positions, however, remain unchanged. We are interested first of all in the subsequent dynamics of the future FS.

Let us introduce definitions of several parameters used in the sequel (Figure 2), namely:

1) position R_{FS} of the maximum difference brightness ΔP_{FS};

2) position R_b of the FS leading part, which is determined by the intersection of the straight line approximating points of the FS front with the *R*-axis.

In addition, we are interested in the time period Δt_{FS} during which the initial position R_{FS}=1.028$R_\odot$ of the ΔP_{FS} maximum remains unchanged. According to Figure 2, *b*, $\Delta t_{FS} \approx 4 \pm 1$ min. After 17:40:11 UT (open triangles), FS begins to move (see the next instant 17:40:35 UT (diamonds) and further in Figure 2, *c*).

The initial position of the FS leading part R_b=1.037$R_\odot$ (crosses in Figure 2, *a*). Position of the leading part begins

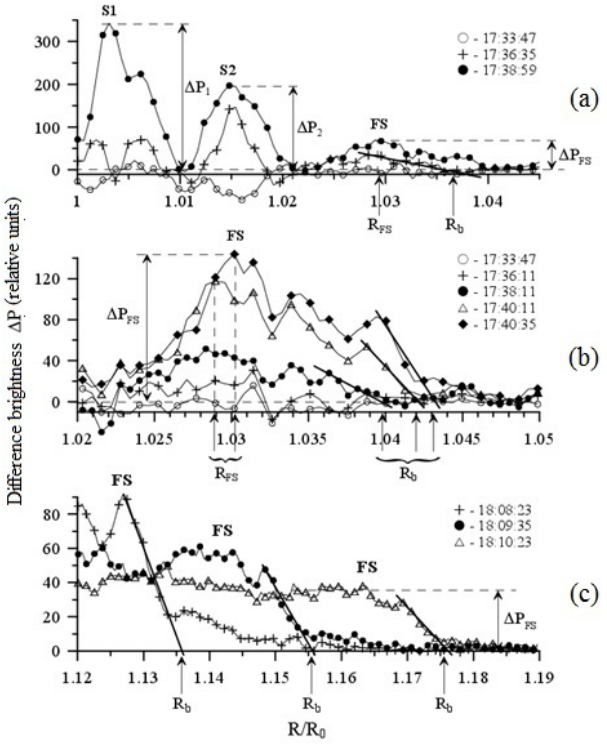

Figure 2. Distributions of the difference brightness $\Delta P(R)$ in the 131 Å channel at t_0=17:30:11 UT plotted in the direction PA=300° (dashed line in Figure 1) for successive instants of time on January 27, 2012. SDO/AIA data

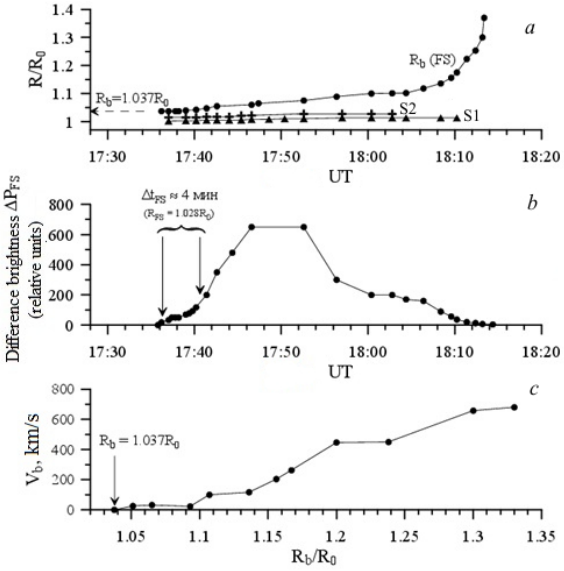

Figure 3. Time dependences of positions R of the structures S1 (black triangles), S2 (crosses) relative to the center of the Sun, positions R_b of the FS leading part (black circles) (*a*); of the FS maximum difference brightness ΔP_{FS}, two vertical arrows mark the time period Δt_{FS} during which the position R_{FS}=1.028$R_\odot$ remains unchanged (*b*); dependence of the velocity of the FS leading part on its distance R_b from the Sun, the vertical arrow shows the initial position R_b of the FS leading part at rest (*c*). AIA/SDO data: 131 Å channel, January 27, 2012.

to change earlier than R_{FS} after 17:36:35 UT (black circles in Figure 2, *a*). It is obvious that the movements of R_{FS} and R_b are connected with processes inside the FS arched structure. In this case, before ≈17:40:11 UT, a shift in R_b reflects a broadening of the structure, whereas the movement of R_{FS} after 17:40:11 UT indicates a shift in FS as a whole.

Kinematic dependences $R(t)$ for S1, S2, and FS $R_{FS}(t)$, $R_b(t)$, plotted from $\Delta P(R)$ distributions for different successive instants of time (see Figure 2), are shown in Figure 3, *a*. The structures S1 (black triangles) and S2 (crosses) are seen to oscillate, although slightly, throughout the development of the process up to 18:10 UT, but as a whole remain almost stationary. The position of the ΔP_{FS} maximum, as noted above, remains unchanged for t≈ 4 min (shown by two vertical arrows in Figure 3, *b*): R_{FS}=1.028$R_\odot$. In this case, the position R_b of the FS leading part (black circles) begins to change even earlier, immediately after 17:40 UT, and after 18:10 UT the rate of the changes sharply increases. The difference brightness ΔP_{FS} here first increases and then, after 17:55 UT, begins to rapidly decrease. The greatest decrease in ΔP_{FS} occurs after 18:05 UT (Figure 3, *b*) in the region of maximum acceleration of FS (Figure 3, *a*).

Figure 3, *c* plots the velocity $V_b(R)$ calculated by the formula $V_b(R)=(R_b(t_{i+1})-R_b(t_i))/(t_{i+1}-t_i)$, using the dependence $R_b(t)$ (see Figure 3, *a*). Here, the numerator is the difference between adjacent points along the Y-axis in Figure 3, *a*; the denominator is the time interval between them. Referring to Figure 3, *c*, after a gradual increase in velocity from zero a noticeable acceleration of the leading part occurs at distances R≥1.1$R_\odot$ (at t ≥ 18:10 UT in Figure 3, *a*) and reaches its peak velocity V_{bmax} ≈ 680 km/s in the SDO/AIA field of view (R≈1.35$R_\odot$). In this case, the average velocity of the leading part of this type 1 CME at distances R≈(2÷30)$R_\odot$ V_{av} ≈ 2509 km/s (see Table), according to the data from [http://cdaw.gsfc.nasa.gov/CME_list]

All this suggests that the main processes leading to the formation of the type 1 CME under study take place mainly in the FS outer shell.

2.2. Type 1 CME in the July 19, 2012 event

Let us delve into the type 1 CME whose FS is formed, unlike the January 27, 2012 CME, at a maximum distance from the solar surface accessible to observation by SDO/AIA. This event occurred in the active region NOAA 11520 on July 19, 2012 and was accompanied by an M7.7 X-ray flare with coordinates S13W88, which began at ≈04:20 UT.

Figure 4 presents difference brightness images (at t_0=04:15:10 UT) of the development of this F-CME for successive instants of time. As for the January 27, 2012 CME, we use images in the 131 Å channel since the development of the July 19, 2012 CME at the initial stage is most clearly seen in it.

From Figure 4 *a*–*c* it follows that by 04:25:22 UT two arched structures S1 and S2 become visible at first, and by 04:32:22 and 04:45:46 UT the FS external structure also becomes visible (see Figure 4, *b*, *c*), which is a basis for the future frontal structure of the type 1 CME. The entire set of these structures may be the cross section of a three-dimensional magnetic flux rope filled with plasma, whose footpoints are in the photosphere

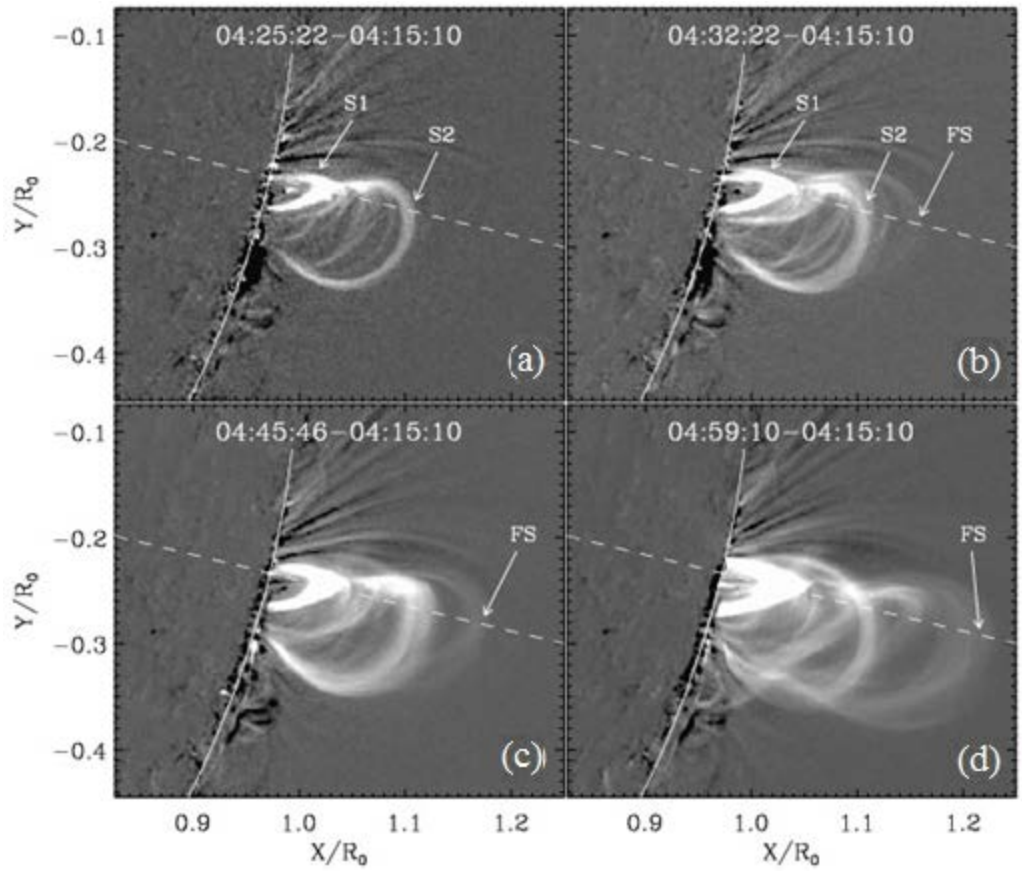

Figure 4. Difference brightness images of type 1 CME development for successive instants of time on July 19, 2012 (according to SDO/AIA data in the 131 Å channel). Positive estimate from the center of the Sun along the Y-axis is to the north, along the X axis, to the west. The distances are normalized to the solar radius $R_\odot$. The dashed line indicates the direction *PA*=256.5°

[Patsourakos et al., 2013]. With time the brightness of S1, S2, and FS increases. After 04:45:46 UT (Figure 4, *c*), FS starts moving away from the Sun, or flux rope eruption begins.

To explore the dynamics of this event, we have plotted the difference brightness distributions ΔP (at t_0 =04:15:10 UT) as a function of the distance R from the center of the Sun for a number of successive instants of time (Figure 5). The distributions are plotted in the direction of the position angle *PA*=265.5°.

Figure 5 *a*, *b* indicates that between 04:33:10 (open circles) and 04:39:58 UT (solid circles) the difference brightness of the S1, S2 structures and FS increases up to ΔP_1, ΔP_2, ΔP_{FS} respectively, their positions remaining virtually unchanged. As in the January 27, 2012 event, we are primarily interested in the dynamics of the future frontal structure. Figure 5, *c* shows initial positions R_{FS}=1.187$R_\odot$ of the maximum difference brightness ΔP_{FS} and R_b=1.213 $R_\odot$ of the FS leading part. Figure 5, *c* suggests that between 04:30:46 (open circles) and 04:39:58 UT (crosses) R_{FS} remains unchanged, so we can assume (accurate to one minute) that Δt_{FS}≈10±1 min.

After 04:39:58 UT, FS begins to move (see the next moment 04:42:22 UT (open triangles) and further (black triangles)). Position of the FS leading part (crosses in Figure 5, *c*) begins to change approximately at the same time as the position of the FS maximum, i.e. after 04:39:58 UT

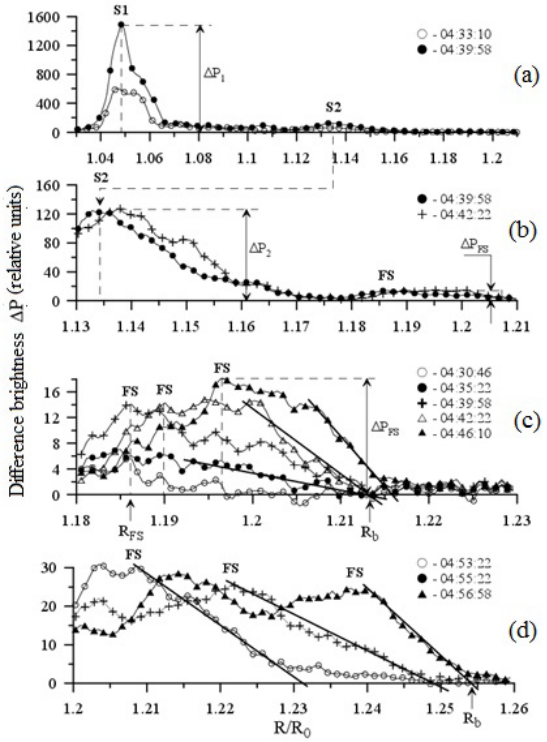

Figure 5. Difference brightness distributions $\Delta P(R)$ in the 131 Å channel at t_0=04:15:10 UT, plotted in the direction *PA* =256.5° (dashed straight line in Figure 4) for successive instants of time on July 19, 2012 (SDO/AIA data)

Thus, the frontal structure begins to move as a whole. Obviously, the movement of R_{FS} and R_b is related to the processes occurring inside the FS arched structure.

The kinematic dependences $R(t)$ for the S1, S2 structures and the FS leading part $R_b(t)$, plotted from the distributions of $\Delta P(R)$ for different successive instants of time (see Figure 5), are shown in Figure 6, *a*. The time dependence of the maximum difference brightness ΔP_{FS} is shown in Figure 6, *b*. The distance dependence of the velocity $V_b(R)$ of the FS leading part, plotted using the dependence $R_b(t)$ (Figure 6, *a*) from the formula given in Section 2.1, is displayed in Figure 6, *c*.

Let us compare these dependences for the type 1 CMEs on July 19, 2012 (Figure 6) and January 27, 2012 (Figure 3). What do they have in common and what are the differences? These events are similar in:

1) practical invariability of positions of the internal structures S1 (black triangles), S2 (crosses) throughout the development of the process;

2) acceleration and, accordingly, eruption of only the external arched structure of FS, which then is a basis for the future frontal structure of the type 1 CME;

3) existence of the time interval Δt_{FS} before the acceleration of the FS external structure, during which the maximum brightness ΔP_{FS} of the structure increases, and the position R_{FS} remains practically unchanged.

The main differences between these events:

1. Initial positions of the maximum difference brightness ΔP_{FS} and the FS leading part in the July 19, 2012 event R_{FS}=1.187$R_\odot$ and R_b=1.213$R_\odot$ respectively. In the January 27, 2012 event, these initial positions were noticeably closer to the Sun: R_{FS}=1.027$R_\odot$ and R_b=1.037$R_\odot$ (see Figure 6, *b*, *c*).

2. The time interval Δt_{FS} during which FS remains stationary with increasing brightness is ≈10 ± 1 min for the July 19, 2012 CME (see Figure 6, *b*). For the January 27, 2012 CME, Δt_{FS} is two or more times less, 4±1 min.

3. The maximum velocity $V_{b\,max}$ of the leading part, recorded in the SDO/AIA field of view, is ≈102 km/s for the July 19, 2012 CME and ≈680 km/s for the January 27, 2012 CME (see Table).

4. The average (linearly averaged) velocity V_{av} of the leading part at distances R≈(2–30)$R_\odot$ is ≈1630 km/s for the July 19, 2012 CME and ≈2509 km/s for the January 27, 2012 CME (see Table).

In addition to the CMEs presented above, we have studied three more limb type 1 CMEs (F-CMEs) in a similar way. These are the events of September 22, 2011, September 10, 2017, and June 23, 2012 (see Table). The initial positions R_{FS} and R_b for these CMEs were intermediate between values for the July 19, 2012 and January 27, 2012 CMEs. As noted above, the external arched structure of FS of limb type 1 CMEs is the outer boundary of the cross section of the magnetic flux rope whose footpoints are in the photosphere. In this case, the arched structures such as S1, S2, etc. inside FS, if any, can both be an integral part of the cross section of the magnetic flux rope and be located near the ejection region and projected to the common region of the plane of the limb.

In the three type 1 CMEs considered, the number

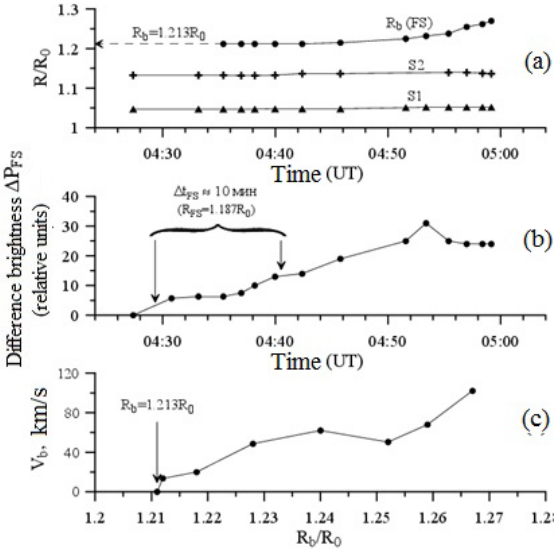

Figure 6. Time dependences of positions R and R_b of structures S1 (black triangles) and S2 (crosses) and the FS leading part (black circles) relative to the center of the Sun (*a*); maximum difference brightness ΔP_{FS} of the frontal structure; two vertical arrows indicate the time period Δt_{FS} during which the position R_{FS}=1.187 $R_\odot$ remains unchanged (*b*); the FS leading part velocity as a function of its distance R_b from the Sun (*c*); the vertical arrow denotes the initial position R_b of the FS leading part. AIA/SDO data, 131 Å channel, July 19, 2012.

of these structures was different: 0 in the June 23, 2012 event, 2 in the September 10, 2017 event, and 5 in the September 22, 2011 event. These differences in the internal cross section of the magnetic flux rope are associated with features of the active region above/in which it is formed, and do not fundamentally affect the eruption of the FS external structure.

2.3. Generalization of type 1 CME features

Generalizing plots (Figure 7) for five F-CMEs (black circles) allow us to draw a number of conclusions about some of their general properties.

First of all, from Figure 7, *a* it follows that the closer the formation of CMEs to the solar surface, the greater the maximum velocity $V_{b\,max}$ the type 1 CME leading part (black circles) achieves in the SDO/AIA field of view (i.e. at R<1.4 $R_\odot$). This dependence unambiguously refutes the previously existing classification of CMEs into impulsive and gradual, which would be formed in the corona at distances R>1.1$R_\odot$ from the center of the Sun [Sheeley et al., 1999]. However, by the example of the five events considered, which we have classified as type 1 CMEs, we can conclude that they have a common nature. Note that for the events of interest the lower the type 1 CME is formed the greater the average velocity V_{av} at distances 2$R_\odot$<R<30 $R_\odot$ (Table, columns 3 and 4), as derived from LASCO C2 and C3 data [http://cdaw.gsfc.nasa.gov/CME_list].

The closer the formation of type 1 CME to the solar surface, the faster it is formed, i.e. the shorter the time interval Δt_{FS} (Figure 7, *c*) and the greater the maximum velocity $V_{b\,max}$ of the FS leading part at R<1.4 $R_\odot$ (Figure 7, *b*).

3. TYPE 2 CME VELOCITY DEPENDENCE ON DISTANCE,WHERE ITS LEADING PART IS FORMED

Let us carry out a similar analysis for two limb CMEs of a different type, namely, the CMEs associated with eruptive prominences, or type 2 CMEs, using the August 24, 2014 and February 25, 2014 events, which have been analyzed in detail in [Eselevich et al., 2016; Eselevich, Eselevich, 2020] as an example. By an eruptive prominence is meant a magnetic flux rope with a core of cold (T<6000–10000 K) plasma, which was at rest above the photosphere prior to the event. In this case, the following two variants are possible:

1. An active prominence that is a magnetic flux rope in the active region and remains invisible until activation process begins in it. With the onset of activation, brightness of the flux rope increases and it becomes visible, primarily in the cold channels 6562.8 (Hα), 1700, 304 Å, etc., as well as in some hotter channels (193 Å, etc.), and then erupts.

2. An ordinary prominence that before the activation is seen on the solar disk in the 6562.8 Å (Hα) channel as a region of reduced brightness and is a magnetic flux rope with plasma at T< 6000–10000 K. With the beginning of activation, its brightness also increases in all the above channels, and then it erupts.

The former case includes the August 24, 2014 CME; the latter, the February 25, 2014 CME. Both events are designated as type 2 CMEs, i.e. associated with an eruptive prominence. Since the essence of both type 2 CMEs is the same, and the events themselves have been analyzed in detail in [Eselevich et al., 2016; Eselevich, Eselevich, 2020], here we take a brief look only at the August 24, 2014 event to illustrate the differences and reasons for the classification into type 1 and type 2 CMEs.

3.1. Type 2 CME in the August 24, 2014 event

The type 2 CME of interest occurred in the active region NOAA 12151 with coordinates S07 and >E60 and was accompanied by an M5.9 class flare with heliographic coordinates S07E78, which began at ≈12:00 UT. Thus, on August 24, 2014, the type 2 CME was in the visible part of the disk close to the limb.

Let us briefly compare the dynamics of the type 2 CMEs, using running difference brightness images in the cold channel 1700 Å ($T\approx5\cdot10^3$ K) and the hotter channel 193 Å (with two temperature maxima $T\approx1.6\cdot10^6$ K and $\approx2\cdot10^7$ K). The development of this CME has been analyzed in more detail in [Eselevich et al., 2016].

In the 1700 Å channel from 12:08:07 UT (Figure 8, *a–d*), an expanding bright arched structure (shell) appears near the solar surface and moves approximately along the radial direction. According to the analysis carried out in [Eselevich et al., 2016], this arched structure is a characteristic cross section of a magnetic flux rope filled with cold plasma (T< 6000 K). The flux rope was initially invisible and was located near the photosphere at 400–600 km, corresponding to the minimum

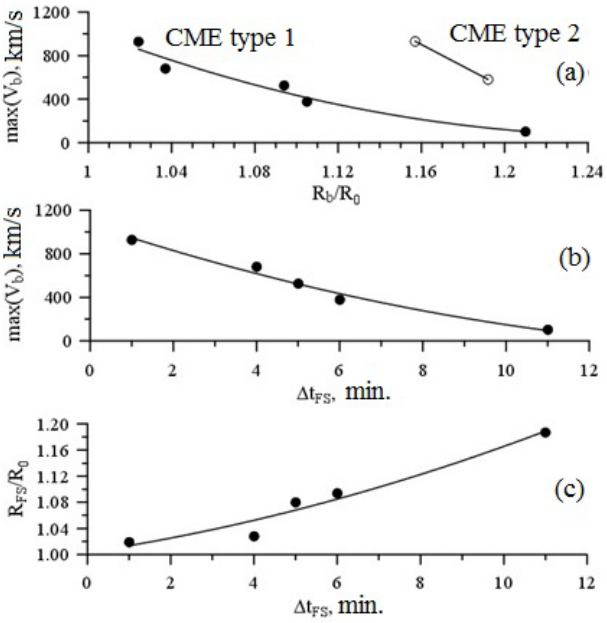

Figure 7. Maximum velocity $V_{b\ max}$ of the leading part of type 1 CME (black circles) and type 2 CME associated with eruptive prominences (open circles), recorded in the SDO/AIA field of view, as a function of the initial position $R_b/R_\odot$ of the FS leading part (*a*) and the time interval Δt_{FS} during which FS remains stationary (*b*). Position R_{FS} of maximum difference brightness ΔP_{FS} as a function of Δt_{FS} (*c*). Experimental points are approximated by a parabola

temperature of photospheric plasma. In Figure 8, *a–d*, the flux rope is denoted as EP — eruptive prominence.

Figure 8, *e–h* presents running difference brightness images in the 193 Å hot channel for four successive instants of time, which show the development of this event. The dashed line indicates the position angle PA=101°. The fundamental difference between the development of an ejection in the hot channel 193 Å and the cold channel 1700 Å is the existence of two interrelated processes with different locations. The first process begins after ≈12:08:07 UT on August 24, 2014, and is associated with an increase in brightness near the solar surface and the EP eruption, analyzed above using 1700 Å channel data. The second process begins almost simultaneously with the start of EP formation, but at a greater distance from the Sun. In the images presented in Figure 8, *f–h*, it reveals itself as an increase in the brightness of several nested arched structures of a larger scale than EP. The set of these structures is conventionally designated as S1 in Figure 8, *f*. In Figure 8, *g*, a more distant structure S2, which became visible due to the increase in brightness, is added to them. These structures represent an inner cross section of a magnetic flux rope larger than EP, whose footpoints are in the photosphere at the edge of AR 12151, similarly to that observed in [Patsourakos et al., 2013].

To take a closer look at the formation of arched structures and their dynamics, Figure 9 shows distributions of the running difference brightness ΔP_R (R) in the 193 Å channel, which are plotted in the direction of the position angle PA≈101° for successive instants of time. The sequence of curves on the left in Figure 9 *a–c* reflects

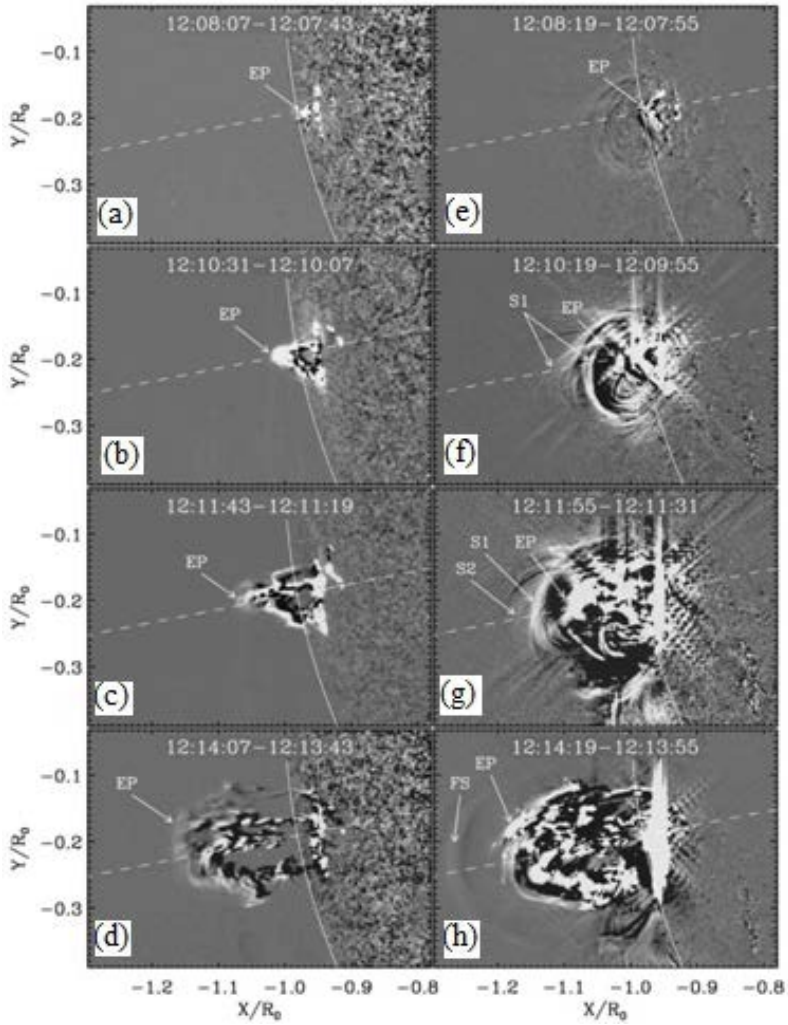

Figure 8. Difference images of the development of type 2 CMEs at successive instants of time in the 1700 Å (*a*–*d*) and 193 Å (*e*–*h*) channels, according to SDO/AIA data. August 24, 2014 event

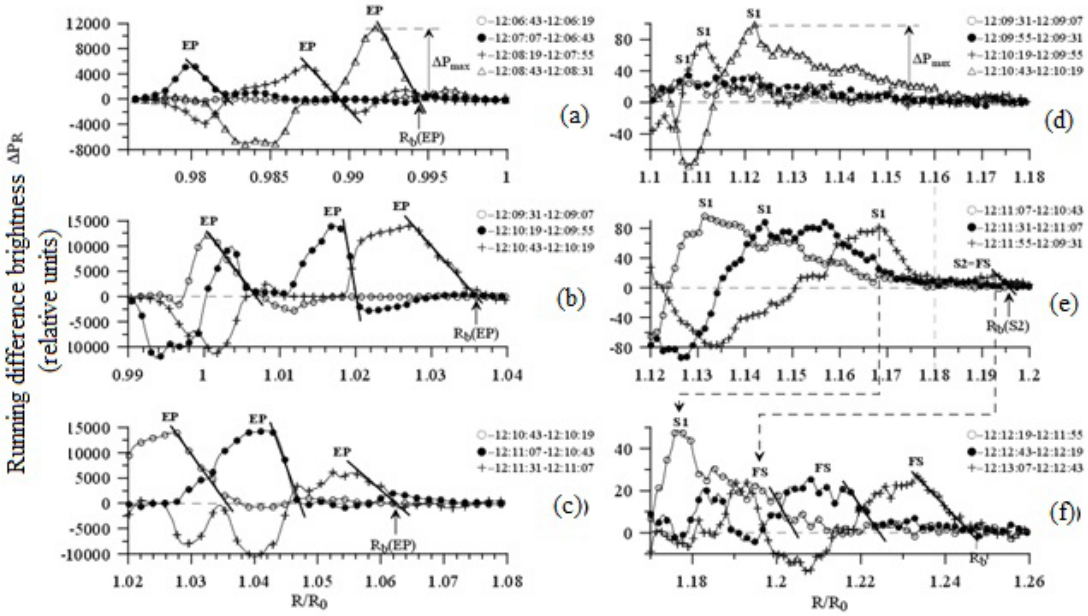

Figure 9. Distributions of running difference brightness $\Delta P_R(R)$ in the 193 Å channel plotted in the direction *PA*=101° (dashed line from the center of the Sun in Figure 8) for successive time points on August 24, 2014: for an eruptive prominence EP near the solar surface (*a*–*c*); for arched structures in the solar corona whose merging leads to the formation of FS of this type 2 CME (according to SDO/AIA data) (*d*–*f*)

the temporal dynamics of EP whose maximum brightness ΔP_{max} is indicated by the vertical arrow labeled EP. The position R_b (EP) of the EP leading part is determined by the intersection of the straight line approximating the EP front with the R-axis (Figure 9, *a–c*).

The EP dynamics in the cold channel 1700 Å (omitted here) looks roughly the same. This is due to the fact that when the EP moves, its outer shell (or leading part) heats up more strongly than the inner part (i.e. it becomes visible in the 193 Å channel), and they move as a single whole (see Figure 3 in [Eselevich et al., 2016]).

Figure 9, *a* indicates that the EP maximum brightness ΔP_{max} first increases, and it shifts in the radial direction. Then, after 12:11:07 UT, the maximum brightness begins to sharply decrease (see Figure 9, *c*, black circles and crosses). Eselevich et al. [2016] have shown that here an explosive expansion of EP occurs during which it catches up, traps, and accelerates the large-scale arched structures located in its path.

This process eventually leads to the formation of the frontal structure of EP-CME. The final stage of FS formation is defined by the dynamics of the S1 and S2 structures (see Figure 9, *e*, crosses) whose merging is seen in Figure 9, *f* (open circles). At the same time, S2 becomes a basis for the future FS of the type 2 CME whose maximum brightness at the time of its occurrence was at $R_{max}(S2) \approx 1.193 R_\odot$ (crosses in Figure 9, *e*).

Thus, when observed near the solar limb, the formation of a type 2 CME, in contrast to the formation of a type 1 CME, has the following two stages:

1) ejection and explosive expansion of a prominence (containing cold plasma and an outer shell with rarefied and more heated plasma) whose cross section on the limb is observed as a series of arched structures;

2) acceleration under the action of an expanding prominence of the surrounding arched structures (filled with hotter plasma), which are the cross section of magnetic flux ropes, and their merging followed by the formation of the future frontal structure of type 2 CME.

The process develops similarly during the February 25, 2014 event as well [Eselevich, Eselevich, 2020].

The dependence $V_b(R_b)$ of the leading part of the type 2 CME for these events is shown in Figure 7, *a* by open circles. At the same time, the leading part of type 2 CMEs that form close enough to the solar surface at $R_b/R_\odot \approx 1.165$, can at large distances $R \approx (2 \div 30) R_\odot$ have average velocities V_{av} comparable to those of type 1 CMEs at these distances (see column 3 in Table 1 for the September 22, 2011, January 27, 2012, and February 25, 2014 events). Table (cf. columns 3 and 7) also indicates that the type 2 CMEs considered almost complete their acceleration at distances $R < 1.22\ R_\odot$, whereas type 1 CMEs continue to gain speed outside the SDO/AIA field of view (at $R > \sim 1.2 R_\odot$).

CONCLUSIONS

The analysis of seven limb CMEs has shown that according to features of the development at distances $R < 1.4\ R_\odot$ from the center of the Sun, CMEs can be classified into two types. The features of the formation of CMEs of these types are as follows.

1. In the case of type 1 CME, the frontal structure is formed due to the processes occurring inside the FS itself, which is the outer shell of magnetic flux rope. In this case, internal arched structures of the magnetic flux rope do not affect the formation of FS.

2. The closer to the solar surface a type 1 CME is formed, the faster it moves and the greater the maximum velocity $V_{b\ max}$ the CME leading part attains in the SDO/AIA field of view (i.e. at $R < 1.4\ R_\odot$).

3. As for type 2 CMEs, internal arched structures erupt which expand explosively, capture and accelerate the surrounding more distant arched structures whose merging produces the frontal structure of the type 2 CME.

4. At large distances $R \approx (2–30) R_\odot$, type 1 and type 2 CMEs have comparable average velocities V_{av}.

The results disprove the earlier classification of CMEs into impulsive and gradual [Sheeley et al., 1999], whose frontal structure in the corona would form at distances $R > 1.1\ R_\odot$ from the center of the Sun.

Note that both type 1 and type 2 CMEs are accompanied by solar flares — an increase in electromagnetic (in particular X-ray) radiation fluxes. In this sense, both CME types may be considered flare-associated. In this case, both type 1 and type 2 CMEs are connected with the magnetic flux rope eruption. The difference is that in the case of type 2 CMEs (EP-CMEs) the core of the magnetic flux rope contains cold ($T <$ 6000–10000 K) plasma, whereas type 1 CMEs have no such plasma population. In the future, it seems interesting to figure out what mechanisms are responsible for the appearance of cold plasma in magnetic flux ropes and why this affects the formation of the CME frontal structure.

In conclusion, we add that in this work we have examined only two type 2 CMEs (explored by us earlier), whose formation was observed by SDO/AIA in EUV at low coronal heights ($R_b < 1.22\ R_\odot$). In the future, a larger number of type 2 CMEs are worth analyzing; in particular to supplement our findings with a study of the dynamics of type 2 CMEs associated with prominences whose eruption begins at higher coronal heights ($R_b > 1.22\ R_\odot$).

We thank the SDO/AIA (NASA) space experiment team for the observational data used in this work. We are also grateful to the SOHO/LASCO CME catalog development team: “This CME catalog is generated and maintained at the CDAW Data Center by NASA and The Catholic University of America in cooperation with the Naval Research Laboratory. SOHO is a project of international cooperation between ESA and NASA.” The work was performed with financial support from the Ministry of Science and Higher Education of the Russian Federation (V.G. Eselevich, M.V. Eselevich) and under the Government Assignment "PLASMA" (I.V. Zimovets).

REFERENCES

Alekseenko S.V., Dudnikova G.I., Romanov V.A., Romanov D.V., Romanov K.V. Magnetic field instabilities in the Solar convective zone. *Russian J. Engineering Thermophysics*. 2000, vol. 10, pp. 243–262.

Amari T., Luciani J.F., Mikic Z., Linker J. A twist flux rope model for coronal mass ejections and two-ribbon flare. *Astrophys. J.* 2000, vol. 529, pp. L49–L52. DOI: 10.1086/312444.

Antiochos S.K., DeVore C.R., Klimchuk J.A. A model for solar coronal mass ejections. *Astrophys. J*. 1999, vol. 510, pp. 485–493. DOI: 10.1086/306563.

Archontis V., Hood A.W. A flux emergence model for solar eruptions. *Astrophys. J*. 2008, vol. 674, pp. L113–L116. DOI: 10.1086/529377.

Bemporad A., Raymond J., Poletto G., Romoli M. A comprehensive study of the initiation and early evolution of a coronal mass ejection from ultraviolet and white-light data. *Astrophys. J*. 2007, vol. 655, pp. 576–590. DOI: 10.1086/509569.

Chen H., Zhang J., Cheng X., Ma S., Yang S., Li T. Direct observations of tether-cutting reconnection during a major solar event from 2014 February 24 to 25. *Astrophys. J. Lett*. 2014, vol. 797, article id. L15.

Eselevich V.G., Eselevich M.V. On the Formation Mechanism of the Sporadic Solar Wind. *Geomagnetism and Aeronomy*. 2011, vol. 51, no. 8, pp. 1083–1094.

Eselevich V.G., Eselevich M.V., Romanov V.A., Romanov D.V., Romanov K.V., Kucherov N.V. Physical mechanism for the generation of the coronal mass ejections from the upper layers of the convective zone. *Izvestiya Krymskoj Astrofizicheskoj Observatorii*. 2013, vol. 109, no. 4, pp. 54–60. (In Russian).

Eselevich V.G., Eselevich M.V. Physical differences between the initial phase of the formation of two types of coronal mass ejections. *Astronomicheskii Zhurnal* [Astronomy Reports]. 2014, vol. 91, no. 4, pp. 320–331. (In Russian).

Eselevich V.G., Eselevich M.V., Zimovets I.V., Rudenko G.V. Study of the initial formation stage of an impulsive coronal mass ejection. *Astronomicheskii Zhurnal* [Astronomy Reports]. 2016, vol. 93, no. 11, pp. 990–1002. (In Russian).

Eselevich V.G., Eselevich M.V. Features of the initial stage of formation of fast coronal mass ejection on February 25, 2014. *Solnechno-Zemnaya Fizika* [Solar-Terrestrial Physics]. 2020, vol. 6, no. 3, pp. 3–17. (In Russian).

Gibson S. E., Foster D., Burkepile J., de Toma G., Stanger A. The calm before the storm: the link between quiescent cavities and coronal mass ejections. *Astrophys. J*. 2006, vol. 641. pp. 590–605. DOI: 10.1086/500446.

Hundhausen A.J. Coronal mass ejections. *The Many Faces of the Sun: A Summary of the Results from NASA's Solar Maximum Mission*. New York, Springer, 1999, pp. 143–200.

Kliem B., Titov V.S., Török T. Formation of current sheets and sigmoidal structure by the kink instability of a magnetic loop. *Astron. Astrophys*. 2004, vol. 413, pp. L23–L26. DOI: 10.1051/0004-6361:20031690.

Kliem B., Török T. Torus instability. *Phys. Rev. Lett*. 2006, vol. 96, iss. 25, id. 255002. DOI: 10.1103/PhysRevLett.96.255002.

Krall J., Chen J., Santoro R. Drive mechanisms of erupting solar magnetic flux ropes. *Astrophys. J*. 2000, vol. 539, pp. 964–982.DOI: 10.1086/309256.

Lemen J.R., Title A.M., Akin D.J., Boerner P.F., Chou C., Drake J.F., Duncan D.W., et al. The Atmospheric Imaging Assembly (AIA) on the Solar Dynamics Observatory (SDO). *Solar Phys*. 2012, vol. 275, iss. 1-2, pp. 17–40.DOI: 10.1007/s11207-011-9776-8.

MacQueen R.N., Fisher R.R. The kinematic of solar inner coronal transient. *Solar Phys*. 1983, vol. 89, pp. 89–102. DOI: 10.1007/BF00211955.

Magara T., Longcope D.W. Sigmoid structure of an emerging flux tube. *Astrophys. J*. 2001, vol. 559, iss. 1, pp. L55–L59.DOI: 10.1086/323635.

Moore R.L., Sterling A.C., Hudson H.S., Lemen J.R. Onset of the magnetic explosion in solar flares and coronal mass ejections. *Astrophys. J*. 2001, vol. 552, pp. 833–848. DOI: 10.1086/320559.

Moreno-Insertis F., Schussler M., Ferriz-Mas A. Storage of magnetic flux tubes in a convective overshoot. *Astron. Astrophys*. 1992, vol. 264, pp. 686–700.

Patsourakos S., Vourlidas A., Stenborg G. Direct evidence for a fast coronal mass ejection driven by the prior formation and subsequent destabilization of a magnetic flux rope. *Astrophys. J*. 2013, vol. 764, article id. 125. DOI: 10.1088/0004-637X/764/2/125.

Romanov V.A., Romanov D.V., Romanov K.V. Fault of magnetic fields from the dynamo action region into the atmosphere of the Sun. *Astronomicheskii Zhurnal* [Astronomy Reports]. 1993a, vol. 70, pp. 1237–1246. (In Russian).

Romanov V.A., Romanov D.V., Romanov K.V. Fault of magnetic fields from the solar dynamo action region into the relaxation zone. *Astronomicheskii Zhurnal* [Astronomy Reports]. 1993b, vol. 70, pp. 1247–1256. (In Russian).

Schmieder B., Démoulin P., Aulanier G. Solar filament eruptions and their physical role in triggering coronal mass ejections. *Adv. Space Res*. 2013, vol. 51, pp. 1967–1980.DOI: 10.1016/j.asr.2012.12.026.

Sharykin I.N., Zimovets I.V., Myshyakov I.I. Flare Energy Release at the Magnetic Field Polarity Inversion Line during the M1.2 Solar Flare of 2015 March 15. II. Investigation of Photospheric Electric Current and Magnetic Field Variations Using HMI 135 s Vector Magnetograms. *Astrophys. J*. 2020, vol. 893, iss. 2, 159. DOI: 10.3847/1538-4357/ab84ef.

Sheeley N.R. Jr., Walters J.H., Wang Y.-M., Howard R.A. Continuous tracking of coronal outflows: Two kinds of coronal mass ejections. *J. Geophys. Res*. 1999, vol. 104, no. A11, pp. 24739–24768.DOI: 10.1029/1999JA900308.

Shen Y., Liu Y., Su J. Sympathetic partial and full filament eruptions observed in one solar breakout event. *Astrophys. J*. 2012, vol. 750, article id. 12. DOI: 10.1088/0004-637X/750/1/12.

Sterling A.C., Moore R.L. Slow-rise and fast-rise phases of an erupting solar filament, and flare emission onset. *Astrophys. J*. 2005, vol. 630, pp. 1148–1159. DOI: **10.1086/432044.**

Thernisien A., Vourlidas A., Howard R.A. Forward modeling of Coronal Mass Ejection using STEREO/SECCHI data. *Solar Phys*. 2009, vol. 256, pp. 111–130. DOI: 10.1007/s11207-009-9346-5.

Vršnak, B., Sudar D., Ruzdjak D. The CME-flare relationship: Are there really two types of CME? *Astron. Astrophys*. 2005, vol. 435, pp. 1149–1109. DOI: 10.1051/0004-6361:20042166.

Zhang J., Wang J., Deng Y., Wu D. Magnetic Flux Cancellation Associated with the Major Solar Event on 2000 July 14. *Astrophys. J*. 2001, vol. 548, pp. L99–L102. DOI: 10.1086/318934.

Zhang J., Dere K.P. A statistical study of main and residual accelerations of coronal mass ejections. *Astrophys. J*. 2006, vol. 649, pp. 1100–1109. DOI: 10.1086/506903.

URL: http://cdaw.gsfc.nasa.gov/CME_list (accessed 15 December 2021).

Original Russian version: *V.G. Eselevich, M.V. Eselevich, I.V. Zimovets*, published in Solnechno-zemnaya fizika. 2022. Vol. 8. Iss. 2. P. 12–22. DOI: 10.12737/szf-82202202. © 2022 INFRA-M Academic Publishing House (Nauchno-Izdatelskii Tsentr INFRA-M)

How to cite this article

Eselevich V.G., Eselevich M.V., Zimovets I.V. Possible difference in the formation of coronal mass ejections of two types. *Solar-Terrestrial Physics*. 2022. Vol. 8. Iss. 2. P. 10–19. DOI: 10.12737/stp-82202202.